IMAGE ANALYSIS FOR THE AUTOMATED ALIGNMENT OF THE ADVANCED RADIOGRAPHY CAPABBILITY (ARC) DIAGNOSTIC PATH[*]

Randy Roberts[†], Abdul Awwal, Richard Leach, Michael Rushford,
Erlan Bliss and Karl Wilhelmsen,
Lawrence Livermore National Laboratory, Livermore, CA 94550, USA

Abstract

The Advanced Radiographic Capability (ARC) at the National Ignition Facility was developed to produce a sequence of short laser pulses that are used to backlight an imploding fuel capsule. This backlighting capability will enable the creation of a sequence of radiographs during capsule implosion and provide an unprecedented view into the dynamics of the implosion. A critical element of the ARC is the diagnostic instrumentation used to assess the quality of the pulses. Pulses are steered to the diagnostic package through a complex optical path that requires precision alignment. A central component of the alignment system is the image analysis algorithms, which are used to extract information from alignment imagery and provide feedback for the optical alignment control loops. Alignment imagery consists of complex patterns of light resulting from the diffraction of pilot beams around cross-hairs and other fiducials placed in the beam path. This paper describes the alignment imagery for two ARC automated alignment loops, and the image analysis algorithms used to extract information required for the operation of those loops.

INTRODUCTION

Laser pulses produced by the Advanced Radiographic Capability (ARC) at the National Ignition Facility (NIF) require comprehensive characterization to ensure that they meet design specifications. To perform this characterization, selected pulses from the ARC are directed to a diagnostic table containing a variety of instrumentation. The optical path that directs these pulses is complex and requires automated alignment of a large number of optics. The alignment process consists of manipulating mirrors to center and point the beams (pulses) along the optical path. Feedback loops provide inputs to actuators on the mirror mounts, and adjust the actuators to decrease the distance between reference and beam-position fiducials extracted from alignment imagery. Control loops execute two image processing algorithms, one for centering the beam and one for pointing the beam. Imagery for the centering operation is collected by a near-field camera, and imagery associated with pointing operations is collected by a far-field camera.

Figure 1 illustrates a simplified schematic of the beam path from the compressor vessels to the diagnostic table. ARC compressor vessels CV1 and CV2 each compress pulses from two modified NIF beams using arrays of diffraction gratings [1]. NIF beams are directed out of CV1 and CV2 toward the target chamber by the AM5 mirrors. The AM5 mirrors are partially transmitting, allowing 0.2% of each ARC beam and 70% of each pilot beam to propagate to its DM1 mirror. Each DM1 mirror is mounted on a vertical translation stage, which enables it to reflect either the upper or lower output from the associated compressor vessel. After DM1, the beams are reflected by the DM2 mirrors towards calorimeters positioned behind the DM3 mirrors. Beams from CV1 and CV2 are directed by the DM3 mirrors to mirror DM4. This mirror pivots to select the output beam from either CV1 or CV2. From there, a single beam is directed into the diagnostic table by mirrors DM5, DM6 and DM7.

In the ARC diagnostic path, there are three sets of pointing and centering loops that control the DM1/DM2, DM3/DM4 and DM5/DM7 mirror pairs. Near-field and far-field cameras for these loops are positioned respectively behind the DM3, DM5 and on the ARC Diagnostic Table. In this paper, we describe image processing algorithms associated with the DM3/DM4 and DM5/DM7 centering loops. (Space limitations preclude a discussion of all image processing used to align the path from the ARC compressor vessels to the ARC diagnostic table. The DM3/DM4 and DM5/DM7 centering loops were selected for their technical interest.)

Pointing and centering loops DM1/DM2, DM3/DM4 and DM5/DM7 are aligned using small-diameter pilot beams positioned beneath the larger NIF/ARC beams. Three pilot beams are associated with each NIF beam, a 980 nm beam straddled by two 1053 nm beams. These pilot beams propagate alignment references positioned at surveyed locations along the beam path. These cross-hairs and apertures impose patterns on the intensity profiles of the pilot beams which serve as alignment fiducials. For example, cross-hairs beneath the AM5 mirrors identify the correct position for the pilot beams as they pass through. These crosshairs create a diffraction pattern in the pilot beam profiles, and features in this pattern are used in subsequent control loops. As another example, apertures placed beneath the DM5 mirror provide centering references for beams from the CV1 or CV2 compressor vessel for the DM3/DM4 centering loops.

Development of the image processing algorithms and implementation of ARC diagnostic path hardware are pro-
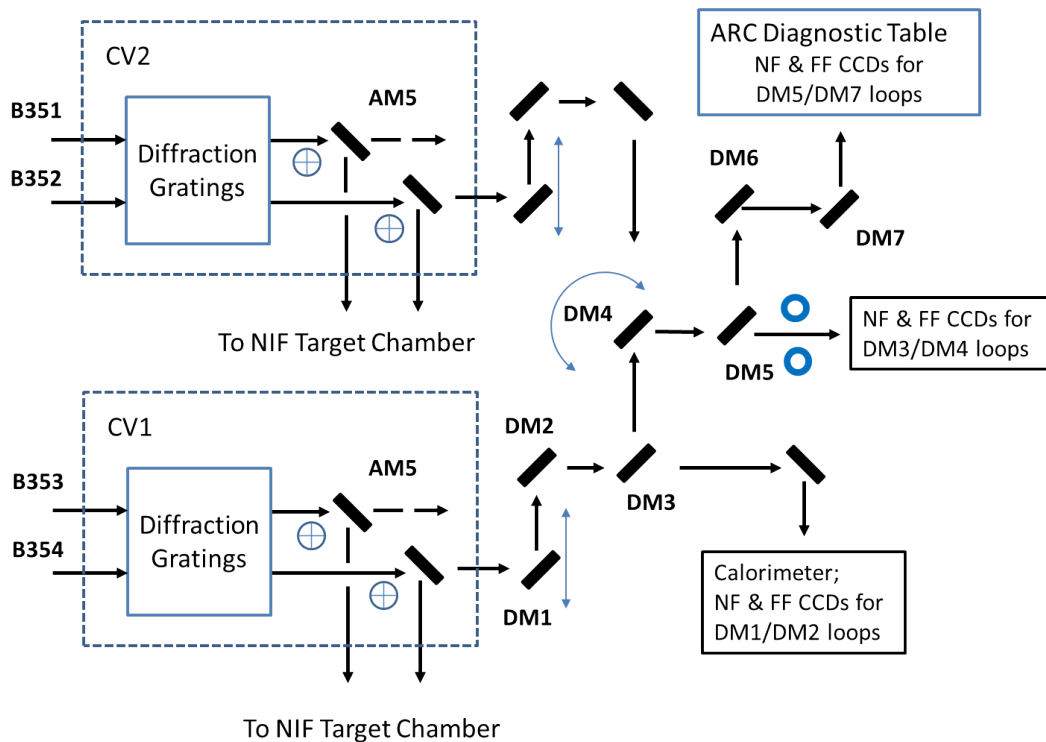

[†] roberts38@llnl.gov

Figure 1: Simplified schematic of the beam path from the ARC compressor vessels to the ARC Diagnostic Table. NIF beams B351 and B352 are input to Compressor Vessel CV1, and beams B353 and B354 input to CV2, and a fraction of one of these beams is switched to the ARC Diagnostic Table. Labels for the DM1—3 mirrors and calorimeter package for CV2 are omitted for clarity.

ceeding in parallel. As a result, imagery from the actual ARC hardware was not available to algorithm developers. To expedite algorithm development, synthetic imagery was created from optical models of the diagnostic path using the FRED Optical Engineering Software [2]. Suites of several hundred images were created for each algorithm to simulate a variety of anticipated beam and optics conditions. The algorithms and imagery presented here, along with all of the image processing algorithms in the diagnostic beam path, were developed using this imagery. When real imagery is available from ARC hardware the image processing algorithms will be appropriately modified as needed.

DM3/DM4 NEAR FIELD IMAGE PROCESSING

A near field image for the DM3/DM4 centering loop is shown in Figure 2a. This imagery, along with imagery for the DM5/DM7 centering loop (presented later), is 1392×1040 pixels and 12-bits deep. Two annuli, one along the pilot beam path from CV1 and the other along the path from CV2, are placed below mirror DM5. These annuli serve as beam centering references. Note that only one annulus is used at a time due to beam selection by DM4. The diffraction pattern from the AM5 crosshair in the 980 nm pilot beam has substantially decreased by this point in the beam path, although some remnants of the pattern remain.
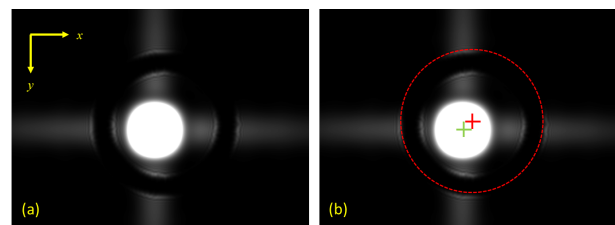

Figure 2: Illustration of the near field image for the DM3/DM4 alignment loop. (a) near field image, (b) near field image annotated with the reference fiducial (red '+') and beam position (green '+').

Image processing is required to estimate the center of the annulus (x_a, y_a) as indicated in Figure 2b by the red '+'. (The exterior edge of the ring is outlined in red for reference.) The image processing is also require to estimate the center of the pilot beam (x_b, y_b), as indicated by the green '+' in Figure 2b. Using these two fiducials, the centering loop manipulates mirrors DM3/DM4 to align the center of one pilot beam (selected by DM4) with the center of its associated annulus.

Processing of the DM3/DM4 near field image I begins with a series of checks to detect off-normal conditions such as excessive saturated pixels, very low contrast image, etc. See [3] for a discussion of off-normal checks. After the im-

age has been screened, a 3×3 Sobel operator is convolved with I to create edge image E. Projections along the x- and y-coordinates are next performed:

$$p_x(j) = \langle E_{ij} \rangle_i \qquad (1)$$
$$p_y(i) = \langle E_{ij} \rangle_j \qquad (2)$$

where, for example, the equation $p_x(j) = \langle E_{ij} \rangle_i$ indicates that the jth entry of the x-projection is found by averaging E_{ij} over the columns that span row j. Edge image E and the x- and y-projections are shown in Figure 3. Projections p_x and p_y are thresholded and the resulting binary sequences are searched for zero-run-lengths that are approximately as long as the number of pixels in the width of the annulus shadow in the DM3/DM4 near field image. Denote the maximum and minimum indices of these zero-run-lengths as x_r, x_l, y_u and y_l to denote the right, left, upper and lower boundaries of the exterior edge of the annulus. These values provide an initial estimate of the radius of the annulus $\tilde{r}_a$, and the average of these values provide an initial estimate of the center of the annulus $(\tilde{x}_a, \tilde{y}_a)$.

The initial estimate of the annulus radius $\tilde{r}_a$ is then used to obtain a more accurate estimate of the center of the annulus. Circles with a range of radii $C(r_i)$ are correlated against the edge detected image, and the radius corresponding to the maximum normalized correlation is selected as the estimate of the location of the annulus center $(\hat{x}_a, \hat{y}_a)$. An estimate of the beam center is provided by a simple weighted average over the interior of the annulus:

$$\hat{x}_b = \frac{\sum_m (\sum_n I(m,n))m}{\sum_m \sum_n I(m,n)}$$
$$\hat{y}_b = \frac{\sum_n (\sum_m I(m,n))n}{\sum_m \sum_y I(m,n)} \qquad (3)$$

where indices m, n are restricted to the interior region of the annulus. The DM3/DM4 near-field image processing algorithm is synopsized in algorithm 1.

Algorithm 1 DM3/DM4 Near Field Image Processing

1: Perform off-normal checks on image I
2: Convolve I with Sobel operator to produce edge image E
3: Average across rows and columns of E to create projections $p_y(\cdot)$ and $p_x(\cdot)$
4: compute rough estimate exterior radius $\tilde{r}_a$ and center $(\tilde{x}_c, \tilde{y}_c)$ of annulus
5: Refine estimate of radius and center of annulus by correlating I with circular kernels $C(r_i)$ over a range of radii r_i
6: Estimate annulus center $(\hat{x}_c, \hat{y}_c)$ as the location of the correlation peak
7: Estimate beam center $(\hat{x}_b, \hat{y}_b)$ as the weighted centroid of the interior region of the annulus
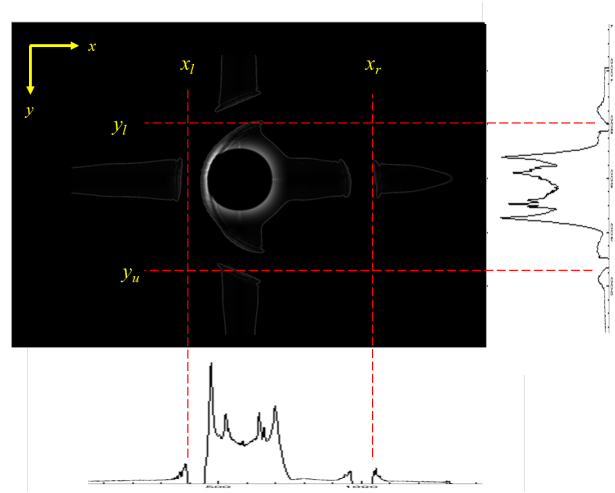

Figure 3: DM3/DM4 near field edge detection image and x- and y-projections of the edges.
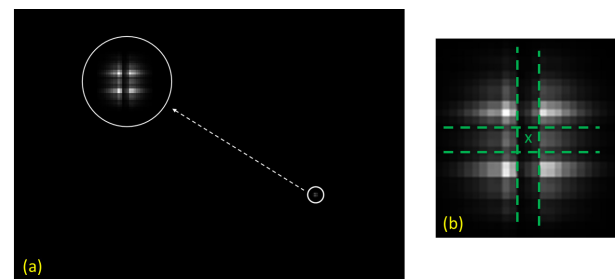

Figure 4: Illustration of the near field image of the DM5/DM7 centering loop. (a) Pattern created by the 1053 nm pilot beam and the AM5 cross-hair. (b) Enlarged view of the pattern annotated with the '+' pattern (green dashed lines) and the center of the pattern (green 'x').

DM5/DM7 NEAR FIELD IMAGE PROCESSING

The near field image of the DM5/DM7 alignment loop is imaged on a camera on the ARC Diagnostic Table and appears as an image of the AM5 crosshair back-lit by the pilot beam. The region of support of the pattern is tiny (approximately 25×25 pixels, see Figure 4a), and an enlargement of the pattern is shown in Figure 4b. The image processing is required to estimate the location of the center of the crosshair. This point is roughly described as the center of the '+' shaped shadow within the illuminated region of the pattern. The centering loop manipulates mirrors DM5/DM7 to align this fiducial with a predefined point on the near field camera.

The DM5/DM7 near field image I is first processed though several off-normal checks as previously described for the DM3/DM4 near field image. After off-normal checks, the image is processed in two steps: an initial estimate of the fiducial location is obtained and then later refined. To begin, image I is converted to binary image B
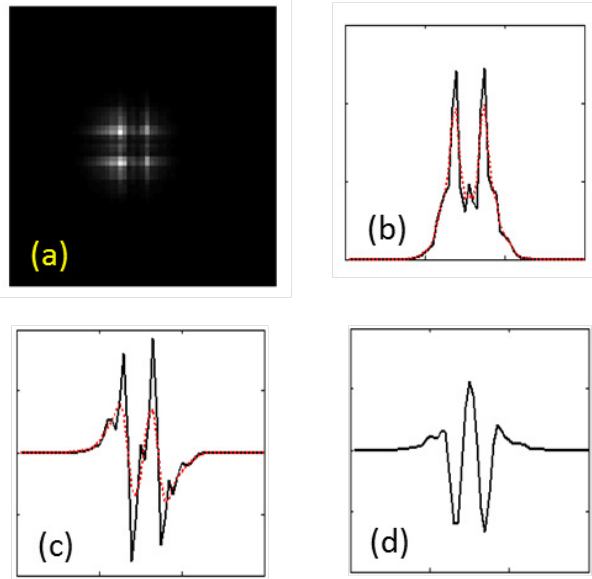
Figure 5: Image processing for the Near field image for the DM5/DM7 centering loop. (a) DM5/DM7 near field image, (b) projection in the x direction (red line indicates smoothed projection), (c) the first (smoothed) difference, (d) second smoothed difference.

by applying a threshold followed by morphological fill operations. The largest connected region R in image B is found, and the weighted centroid $(\tilde{x}_c, \tilde{y}_c)$ of these pixels is computed (cf. Equation 3). A mask is created by defining a circular region large enough to contain the region of support of the pattern centered at $(\tilde{x}_c, \tilde{y}_c)$. Image I is multiplied by this mask to create image M. This completes the calculation of the initial center estimate in the first phase of the algorithm.

In the second phase, $(\tilde{x}_c, \tilde{y}_c)$ is refined by a process of projection and smoothed differencing. The rows and columns of masked image M are projected to form mean projections $p_x(j) = \langle M_{ij} \rangle_i$ and $p_y(i) = \langle M_{ij} \rangle_j$. The projections contain information on the slope of the illumination pattern, which in turn is used used to estimate the location of the fiducial. Each projection is differenced and smoothed twice to provide the second difference of the image projections. For example, the first smoothed-difference p'_y is found from projection p_y as:

$$p'_y = [p_y(1) - p_y(0), \ldots, p_y(N-1) - p_y(N-2))] * W_s \tag{4}$$

where W_s is a smoothing kernel applied to the difference sequence. In a similar manner, second difference p''_y is found from p'_y. The locations of the peaks of the smoothed second-difference projections provide a refined estimate of the fiducial location. See Figure 5 for exemplar plots of the projections.

While many interpolation approaches are available for locating the position of a peak, a simple and robust scheme was used here. The set of indices P is formed from the

smoothed second-difference projections where each index is associated with an amplitude that is greater than threshold $T_a = \sqrt{(2)}/2$ times the peak value in the projection. For example, for the y-projection we have the set of indices:

$$P_y := \{i | p''_y(i) \geq T_a * \max(p''_y(i)\} \tag{5}$$

In this case, the refined estimate of the y-coordinate for the fiducial is average of the indices in set P_y: $\hat{y} = \langle P_y \rangle$. In a similar manner, the estimate for the x-coordinate for the fiducial is found as the average of indices in set P_x: $\hat{x} = \langle P_x \rangle$. The DM5/DM7 near field image processing algorithm is synopsized in Algorithm 2.

Algorithm 2 DM5/DM7 Near Field Image Processing

1: Perform off-normal checks on image I
2: Create binary image: $[I]_T \to B$
3: Locate largest connected region R in image B
4: Calculate weighted centroid of pixels $(\tilde{x}_c, \tilde{y}_c)$ within region $I(R)$
5: Define circle region surrounding $(\tilde{x}_c, \tilde{y}_c)$. Use this region to mask image I and create masked image M
6: Average across rows and columns of M to create projections $p_y(\cdot)$ and $p_x(\cdot)$
7: Compute smoothed difference projections p''_y and p''_x
8: Refine estimate of fiducial location $(\tilde{x}_c, \tilde{y}_c)$ to $(\hat{x}, \hat{y})$ using peak locations in smoothed second difference projections $p_y(\cdot)$ and $p_x(\cdot)$

SUMMARY

We have developed a set of image processing algorithms that are used in control loops that align the beam path from the ARC compressor vessels to the ARC Diagnostic Table. Two of those algorithms were presented here. These algorithms were developed using suites of synthetic imagery created by optics modeling software. Algorithm development using synthetic imagery has allowed us to greatly reduce the amount of time required to deploy the algorithms to hardware. Algorithm performance will be fully assessed when implementation of the ARC diagnostic path hardware is fully implemented and qualified.

REFERENCES

[1] Crane, J. K., et al. "Progress on converting a NIF quad to eight, petawatt beams for advanced radiography." *Journal of Physics: Conference Series*. Vol. 244. No. 3. IOP Publishing, 2010.

[2] "FRED Software." Internet: www.photonengr.com/software/, [9 Sept 2013].

[3] J.V. Candy, et al., "Detection of off-normal images for NIF automatic alignment", in: K. Iftekharuddin, A.A.S. Awwal (Eds.), *Photonic Devices and Algorithms for Computing VII*, Proc. of SPIE, vol. 5907, p.59070B, 2005.